INTERNATIONAL ATOMIC ENERGY AGENCY
UNITED NATIONS EDUCATIONAL, SCIENTIFIC AND CULTURAL ORGANIZATION

INTERNATIONAL CENTRE FOR THEORETICAL PHYSICS
34100 TRIESTE (ITALY) - P.O.B. 586 - MIRAMARE - STRADA COSTIERA 11 - TELEPHONES: 224281/2/3/4/5/6
CABLE: CENTRATOM - TELEX 460392-1

SMR/115 - 2

WINTER COLLEGE ON LASERS, ATOMIC AND MOLECULAR PHYSICS

(21 January - 22 March 1985)

Lecture 2: Wiggle Plane Focusing in Linear Wigglers. Optical Guiding in a Free Electron Laser.

A.M. SESSLER
Lawrence Berkeley Laboratory
University of California
Berkeley, California 94720
U.S.A.

WIGGLE PLANE FOCUSING IN LINEAR WIGGLERS

E. T. Scharlemann

I. INTRODUCTION

An electron beam in a long linear wiggler of conventional design requires some quadrupole focusing in the wiggle plane -- the plane perpendicular to the wiggler magnetic field. For the high-emittance (relative to storage rings) electron beam expected from ATA, quadrupole focusing will seriously degrade the performance of the FEL to be built at ATA; according to FRED, the gain of the FEL will be only a third to a half the gain that a helical wiggler would give, for the same beam brightness and current, and the same wiggler length. Furthermore, the trapping fraction will also be much less than for a helical wiggler, so that merely lengthening the wiggler will not greatly increase the gain. A helical wiggler seems the obvious solution to the problem, but the mechanical difficulties of building a helical wiggler with an adjustable taper for ATA appear prohibitive.

The conventional linear wiggler performs so poorly because of the effect of the quadrupole focusing on the longitudinal electron velocity (see Section II). A simple modification to the shape of the magnet pole faces -- approximate parabolic curvature -- eliminates the need for quadrupole focusing (Section III) and should bring the gain of a linear wiggler FEL up to very close to the gain of a helical wiggler FEL. Numerical simulations by FRED (Section IV) support this hope.

A. M. Sessler
L-321

II. QUADRUPOLE FOCUSING IN A LINEAR WIGGLER

The magnetic field of an ideal linear wiggler is

$$\vec{B} = \frac{mc^2}{e}\, b_0 \left[\hat{y} \cosh k_w y \cos k_w z - \hat{z} \sinh k_w y \sin k_w z\right] , \qquad (1)$$

where k_w is the wiggler wavenumber, and the electron beam propagates in the z-direction. The wiggle motion is in the x-direction: the $\hat{x} - \hat{z}$ plane is therefore the wiggle plane.

This field can be derived from a scalar potential

$$\vec{b} \equiv \frac{e\vec{B}}{mc^2} = -\nabla X \qquad (2)$$

with

$$X = -\frac{b_0}{k_w} \sinh k_w y \cos k_w z \ . \qquad (3)$$

Because the field and potential do not depend on x, there is no focusing of the beam in the x-direction; in the y-direction, however, there is focusing that can be approximately described by the harmonic-oscillator equation[1]:

$$y_i'' \equiv \frac{d^2 y_i}{dz^2} = -k_{\beta y}^2\, y_i \qquad (4)$$

with

$$k_{\beta y} = \frac{b_0}{\sqrt{2}\,\gamma} \ . \qquad (5)$$

The approximation here involves writing

$$\cosh k_w y \simeq 1 + \frac{k_w^2 y^2}{2} \quad . \tag{6}$$

In the same approximation, the wiggle motion is

$$x' = \frac{b_0}{\gamma k_w}\left(1 + \frac{k_w^2 y^2}{2}\right) \sin k_w z \quad ; \tag{7}$$

the wiggle amplitude increases with y, as does B_y.

The wiggler focusing in y has the important property that the longitudinal (dimensionless) velocity $\beta_\parallel$ of an electron, averaged over a wiggle period, remains constant in the electron's betatron orbit. For $\gamma \gg 1$, $\beta_\perp \ll \beta_\parallel$

$$\beta_\parallel \simeq 1 - \frac{1}{2\gamma^2} - \frac{\beta_\perp^2}{2} \tag{8}$$

but

$$\beta_\perp = \hat{x}\ \frac{b_0}{\gamma k_w}\left(1 + \frac{k_w^2 y^2}{2}\right)\sin k_w z + \hat{y}\ y' \quad . \tag{9}$$

where y' is the transverse betatron velocity of the electron. (Betatron motion in x is ignored here; we are only illustrating the properties of wiggler focusing.) We can write

$$y = y_\beta \cos\left(k_{\beta y} z + \phi_y\right) \tag{10}$$

where ϕ_y is an arbitrary betatron phase, to obtain

$$\beta_\perp^2 = \frac{b_0^2}{\gamma^2 k_w^2}\left[1 + k_w^2 y_\beta^2 \cos^2\left(k_{\beta y} z + \phi_{\beta y}\right)\right] \sin^2 k_w z$$

$$+ y_\beta^2 k_{\beta y}^2 \sin^2\left(k_\beta z + \phi_{\beta y}\right) \quad . \tag{11}$$

Averaging over a wiggle period ($\sin^2 k_w z \to 1/2$) and using Eq. (5) for $k_{\beta y}$ yields

$$\overline{\beta_\perp^2} = \frac{b_0^2}{2\gamma^2 k_w^2}\left(1 + k_w^2 y_\beta^2\right) \quad . \tag{12}$$

This expression, and hence $\beta_\parallel$, are both constant in z along a betatron orbit.

It is important that $\beta_\parallel$ be constant in z so that an electron can remain nearly resonant with the ponderomotive potential well produced by the wiggler field plus the laser electromagnetic field. The phase of an electron in the ponderomotive potential well is often denoted by ψ, where[2]

$$\psi \equiv (k + k_w) z - \omega t \tag{13}$$

and k and ω are the wavenumber and angular frequency of the laser electromagnetic field. Then

$$\frac{d\psi}{dz} = k + k_w - \frac{k}{\beta_\parallel} \tag{14}$$

$$= k_w - \frac{k}{2\gamma^2} - \frac{\overline{k\beta_\perp^2}}{2}$$

averaged over a wiggle period. If $\overline{\beta_\perp^2}$ is not constant, electrons are periodically pushed around in the ponderomotive well by their betatron motion.

This periodic pushing does occur if electron drifts in the wiggle plane are confined by quadrupolar focusing, for which

$$x_0'' = -k_q^2 x_0$$

$$\text{with} \quad k_q^2 = q_0/\gamma \equiv \frac{e}{mc^2} Q_0/\gamma \quad , \tag{15}$$

Q_0 is the quadrupole strength (the field gradient), and x_0 is the slowly varying position of the guiding center of the electron's wiggle motion. The combination of guiding center harmonic motion with wiggle motion produces

$$x = x_\beta \cos(k_q z + \phi_q) - \frac{b_0}{\gamma k_w^2}\left(1 + \frac{k_w^2 y^2}{2}\right)\cos k_w z \quad . \tag{16}$$

Quadrupole focusing in x defocuses in y; instead of eq. (10), we have

$$y = y_\beta \cos(\tilde{k}_\beta z + \phi_y) \tag{17}$$

with

$$\tilde{k}_\beta^2 = k_{\beta y}^2 - k_q^2 \quad . \tag{18}$$

For $\overline{\beta_\perp^2}$ we now find

$$\overline{\beta_\perp^2} = \frac{b_0^2}{2\gamma^2 k_w^2}\left[1 + k_w^2 y_\beta^2 + \frac{k_q^2}{2}(x_\beta^2 - y_\beta^2)\right]$$

$$+ \frac{k_q^2}{2}\left[y_\beta^2 \sin 2(\tilde{k}_\beta z + \phi_y) - x_\beta^2 \sin 2(k_q z + \phi_q)\right] . \tag{19}$$

The phases ϕ_y and ϕ_q are arbitrary so that the z-dependent term in the square brackets of Eq. (19) cannot, in general, be made to vanish. Therefore, $\beta_\perp^2$ cannot be constant over a betatron orbit; the betatron motion of an electron changes its phase in a ponderomotive potential well, and can detrap the electron. A further discussion can be found in Ref. 3.

For ATA parameters, the phase change occurs on approximately the time scale of a synchrotron oscillation (i.e., non-adiabatically), and with an amplitude $\Delta\psi$ of order unity. FRED says that electrons are rapidly detrapped (Section IV) unless the quadrupole focusing is too weak to keep the electrons within the laser field; if the quadrupole focusing is that weak, then electrons are not trapped at all. According to FRED, for an electron beam current of 2 kA with a brightness[4] $\mathcal{B} \approx 2 \times 10^5$ A cm^{-2}, a helical wiggler on ATA could be expected to have a gain of greater than 7. For identical parameters, a linear wiggler will permit a gain of less than 4.

III. PARABOLIC POLE FACES

The detrapping described in Section II occurs because the $\beta_\parallel$ of an electron depends on its betatron motion in x; e.g., the larger betatron $\beta_\perp$ near $x = 0$ requires a smaller $\beta_\parallel$. The variation in $\beta_\parallel$ does not occur for betatron motion in y because the increase in betatron $\beta_\perp$ near $y = 0$ is precisely compensated by the decrease in wiggle $\beta_\perp$.

We could circumvent the detrapping by betatron motion in x if the wiggle amplitude, hence B_y, increased with $|x|$ as well as with $|y|$. As A. Sessler and J. Wurtele were quick to point out, the increase of B_y with $|x|$ also focuses the electron beam in the wiggle plane. The focusing both removes the

need for quadrupole focusing and keeps $\beta_\perp^2$ constant, as we demonstrate in this section.

The focusing in x occurs for a different reason than the focusing in y (Section II). The y focusing arises from the cross-product of the wiggle motion x' [Eq. (17)] with B_z [Eq. (1)] averaged over a wiggler period. Both x' and B_z have a sin $k_w z$ dependence; their cross-product is proportional to $\sin^2 k_w z$ and has a non-zero average value. The focusing in x, if B_y increases with |x|, is a consequence of the larger x-acceleration by B_y at the outer extents of the wiggle trajectory. Since $\ddot{x} \propto B_y$, and B_y increases with |x|, an electron's acceleration is greatest at the maximum |x| in its wiggle motion - the effect is a net force on the electron toward the y - z plane, where $\bar{x} = 0$.

The focusing force in x follows immediately from a standard analysis of rapidly oscillating motion in a slowly varying field - as found, for example, in Ref. 5. Nevertheless, because of the presence of other components of $\vec{B}$ required by variation of B_y with x, it is useful to analyze the focusing carefully in both x and y. We do this with the magnetic field obtained from

$$x = -\frac{b_0}{k_y} \cosh k_x x \sinh k_y y \cos k_w z \qquad (20)$$

for which

$$\vec{b} = \frac{b_0}{k_y} \left\{ x\, k_x \sinh k_x x \sinh k_y y \cos k_w z + \hat{y}\, k_y \cosh k_x x \cosh k_y y \cos k_w z - \hat{z}\, k_w \cosh k_x x \sinh k_y y \sin k_w z \right\} . \qquad (21)$$

This field is a vacuum solution of Maxwell's equations if

$$k_x^2 + k_y^2 = k_w^2 \quad . \qquad (22)$$

In going from the conventional wiggler field of eq. (1) to eq. (21), we have effectively added a sextupole contribution: the difference of the transverse fields, for small $k_x x$ and $k_y y$, is

$$\Delta b_x = \frac{b_0}{k_y} k_x^2 \, x \, y \qquad (23)$$

$$\Delta b_y = b_0 \left(1 + \frac{k_x^2 x^2}{2} + \frac{k_y^2 y^2}{2}\right) - b_0 \left(1 + \frac{k_w^2 y^2}{2}\right) = b_0 \frac{k_x^2}{2} (x^2 - y^2) \quad . \qquad (24)$$

The difference field is the standard expression for a sextupole.

Sextupole fields are well known to give second-order focusing, with the transverse Lorentz force proportional to a second-order polynomial in x and y. At first glance the focusing in x appears fundamentally different from the focusing in y; however, as will be shown below, the cross term between wiggle motion and guiding center motion of an electron in x gives a harmonic (first order) focusing force on the electron's guiding center.

We are interested in $\overline{\beta_\perp^2}$ and the focusing averaged over a wiggle period, so we examine the focusing by using an averaging method. We assume the position r of an electron can be written

$$\vec{r} = \vec{r}_0 + \vec{r}_1 \qquad (25)$$

where $\vec{r}_1' = (x_1', y_1', z_1')$ varies rapidly -- on a wiggler wavelength, and $\vec{r}_0'$ is constant over a wiggler wavelength, but does vary over a betatron wavelength. $\vec{r}_0$ is the guiding center position of the electron, and $\vec{r}_1$ is the wiggle trajectory.

Furthermore, we will assume that the electron beam is small enough that $k_x x$ and $k_y y$ are small, and relativistic enough that $b_0/\gamma k_w$ is even smaller, so that an expansion in a small parameter is valid. If ϵ is the small parameter of the expansion, then $k_x x$ and $k_y y$ are $\mathcal{O}(\epsilon)$ and $b_0/\gamma k_w$ is $\mathcal{O}(\epsilon^m)$ for $m \geq 2$. The restriction on m merely ensures that $1/\gamma^2$ terms can be neglected with respect to $k_x^2 x^2$ or $k_y^2 y^2$ terms. In practice, for ATA parameters, $m = 2$ and $\epsilon = 0.1$.

The equations of motion for an electron are

$$\ddot{x} = c\left[\dot{z}\frac{b_y}{\gamma} - \dot{y}\frac{b_z}{\gamma}\right] ,$$

$$\ddot{y} = c\left[\dot{x}\frac{b_z}{\gamma} - \dot{z}\frac{b_x}{\gamma}\right] ,$$

$$\ddot{z} = c\left[\dot{y}\frac{b_x}{\gamma} - \dot{x}\frac{b_y}{\gamma}\right] , \qquad (26)$$

with $\vec{b}$ given by Eq. (21). The dot denotes a time-derivative. The dominant terms in the wiggle motion come from

$$\ddot{x}_1 = c\dot{z}_0\frac{b_y}{\gamma} \qquad (27)$$

from which we obtain

$$\dot{x}_1 = c\frac{b_0}{\gamma k_w}\left(1 + \frac{k_x^2 x_0^2}{2} + \frac{k_y^2 y_0^2}{2}\right)\sin k_w z \qquad (28)$$

through $\mathcal{O}(\epsilon^4)$. Equation (28) describes the wiggle motion, which can be seen to increase with both x_0 and y_0.

The other component of the wiggle motion, $\dot{y}_1$, does not vanish; b_x is not zero so an equation analogous to Eq. (27) could be written for $\dot{y}_1$. However, y_1 contributes to focusing and to $\overline{\beta_\perp^2}$ at much higher order than is retained in Eq. (28), and so we neglect y_1 altogether.

To evaluate the focusing, we write (including only the dominant terms)

$$\ddot{x}_0 = \overline{c\dot{z}_0\frac{b_y}{\gamma}} \qquad (29a)$$

$$y_0 = c\left[\overline{x_1\frac{b_z}{\gamma}} - \overline{z_0\frac{b_x}{\gamma}}\right] . \qquad (29b)$$

The averages with $\dot{z}_0$ do not vanish because of the variation of b_y and b_x with x:

$$\ddot{x}_0 = \overline{c^2\dot{z}_0\frac{b_0}{\gamma}\left[1 + \frac{k_x^2(x_0 + x_1)^2}{2} + \frac{k_y^2(y_0 + y_1)^2}{2}\right]\cos k_w z}$$

$$= c^2 z_0\frac{b_0}{\gamma}k_x^2 x_0\,\overline{x_1\cos k_w z} \qquad (30)$$

or

$$\ddot{x}_0 = -\frac{c^2 b_0^2}{2\gamma^2 k_w^2}k_x^2 x_0 \equiv -c^2 k_{\beta x}^2 x_0 \qquad (31)$$

after an average over a wiggle period.

In the same fashion, Eq. (29b) yields

$$\ddot{y}_0 \approx -\frac{(\quad)^2}{2}\, k_y^{\,2}\, y_0 \equiv -\, c^2 k_{\beta y}^{\,2}\, y_0 \quad ; \tag{32}$$

the focusing in y has been decreased by the pole face design because of the $\dot{z}_0 b_x/\gamma$ term in Eq. (29b).

In order to evaluate $\overline{\beta_\perp^{\,2}}$ we need to connect $\ddot{x}_0$, $\ddot{y}_0$ to x_0'' and y_0''. The only subtlety in making the connection can be seen from the identity

$$\ddot{x}_0 = (\dot{z})^2\, x_0'' + \ddot{z}\, x_0' \quad ; \tag{33}$$

the $\ddot{z}\, x_0'$ term is not of higher order than the x_0'' term (K. Halbach, private communication) although the $(\dot{z})^2$ factor can be set to unity. The $\ddot{z}\, x_0'$ term does not, however, contribute to the focusing averaged over a wiggle period, so that we may write

$$x_0'' = -\, k_{\beta x}^{\,2}\, x_0 \quad ,$$

$$y_0'' = -\, k_{\beta y}^{\,2}\, y_0 \quad . \tag{34}$$

From Equations (34), we find

$$x_0 = x_\beta \cos\,(k_{\beta x}\, z + \phi_x) \quad ,$$

$$y_0 = y_\beta \cos\,(k_{\beta y}\, z + \phi_y) \quad , \tag{35}$$

and so

$$\dot{x}_0^{\,2}/c^2 = k_{\beta x}^{\,2}\, x_\beta^{\,2} \sin^2(k_{\beta x} z + \phi_x)$$

$$\dot{y}_0^{\,2}/c^2 = k_{\beta y}^{\,2}\, y_\beta^{\,2} \sin^2(k_{\beta y} z + \phi_y) \quad .$$

For the wiggle motion

$$\overline{\dot{x}_1^{\,2}}/c = \frac{b_0^{\,2}}{2\gamma^2 k_w^{\,2}}\, [1 + k_x^{\,2}\, x_0^{\,2} + k_y^{\,2}\, y_0^{\,2}] \quad ; \tag{37}$$

thus

$$\overline{\beta_\perp^{\,2}} = \overline{x_1^{\,2}}/c^2 + \dot{x}_0^{\,2}/c^2 + \dot{y}_0^{\,2}/c^2$$

$$= \frac{b_0^{\,2}}{2\gamma^2 k_w^{\,2}}\, [1 + k_x^{\,2}\, x_\beta^{\,2} + k_y^{\,2}\, y_\beta^{\,2}] \quad . \tag{38}$$

This is, as advertised, constant for an individual electron over a betatron orbit.

We can get an approximate idea of the shape of the magnet pole face required to generate the field of eq. (21) by the following argument. Assume the field is shaped by steel pole faces (as in a "hybrid" REC-steel wiggler design) and that $\mu \to \infty$ in the steel. At $\cos k_w z = 1$, the steel pole faces should then follow a curve of constant x, so that

$$\cosh k_x x \sinh k_y y = C_0 \quad . \tag{39}$$

The pole face then is approximately parabolic:

$$y(x) = \frac{C_0}{k_y}\left(1 - \frac{k_x^2 x^2}{2}\right) , \tag{40}$$

or, slightly more carefully

$$y(x) = \frac{1}{k_y} \sinh^{-1}\left(\frac{C_0}{\cosh k_x x}\right) . \tag{41}$$

The curve y(x) for $k_x = k_y = k_w/\sqrt{2}$ is shown in Fig. 1; in this case, $k_{\beta x} = k_{\beta y}$ so the x focusing is sufficient to maintain a circular electron beam. It is interesting to note from Fig. 1 that only a small curvature to the pole faces is required to achieve a circular beam.

The $k_x = k_y$ case may not be the optimal way to design the wiggler — cf. D. Prosnitz' scaling arguments (unpublished). He argues there that a ratio of $\sqrt{3}$: 1 for the x : y ratio of an elliptical beam optimizes the trapping fraction, hence potential gain. Fig. 2 shows the pole face shapes needed for that $\sqrt{3}$: 1 ratio; the curvature is marginally perceptible.

IV. NUMERICAL SIMULATIONS OF WIGGLE PLANE FOCUSING

The disastrous effect of quadrupolar focusing on the performance of the ATA FEL was first realized when our 2D numerical simulation code FRED was modified to include i) full betatron motion of the electrons, ii) the treatment of linear wigglers, and iii) quadrupole focusing in the wiggler plane. As mentioned in the introduction, the predicted performance of a linear wiggler was found to be much poorer than a helical wiggler for the same beam energy, current and emittance.

In its current version, the code follows 2000–4000 electrons within one ponderomotive potential well as they move in γ and ψ (longitudinal phase space). The equations that govern the motion in γ and ψ are slightly extended versions of those derived in Ref. 2:

$$\frac{d\gamma_i}{dz} = -e_s \frac{a_w f_B}{\gamma_i} \sin \psi_i$$

$$\frac{d\theta_i}{dz} = k_w - \frac{k}{2\gamma_i^2}\left(1 + a_w^2 + \gamma_i^2 \beta_\perp^2{}_{,\beta} - 2 a_w f_B a_s \cos \psi_i + a_s^2\right) \tag{42}$$

where $a_w \equiv b_0/\sqrt{2}k_w$ for a linear wiggler, e_s is defined below, $a_s \equiv e_s/k$, k is the wavenumber of the laser field, and $\beta_\perp^2{}_{,\beta}$ is the contribution of the betatron motion to $\beta_\perp^2$. The field quantities are all treated as functions of the electron's position (x_i, y_i, z_i), and $\beta_\perp^2{}_{,\beta}$ is evaluated in the electron's betatron orbit.

θ_i is the phase of the electron with respect to a plane electromagnetic wave, propagating with phase velocity equal to c. In terms of the phase in the ponderomotive potential well, ψ_i, and the phase of the electric field ϕ (see below)

$$\theta_i \equiv \psi_i - \phi \quad . \tag{43}$$

The quantity f_B in Eq. (42) is a difference of Bessel functions[6] and differs from unity for a linear wiggler as a consequence of averaging over a wiggler period. For a helical wiggler, $f_B = 1$; for a linear wiggler

$$f_B \equiv J_0(\xi) - J_1(\xi)$$

where (44)

$$\xi \equiv \frac{a_w^2}{2(1+a_w^2)} \quad .$$

The equations for the transverse motion are of the form

$$x_i'' = - k_{\beta x}^2 \, x_i$$

$$y_i'' = - k_{\beta y}^2 \, y_i \qquad (45)$$

with $k_{\beta x}$ and $k_{\beta y}$ functions of z and γ in ways dependent on the specific kind of focusing assumed. For the scheme described in Section III, $k_{\beta x}$ and $k_{\beta y}$ are given by Eqs. (31) and (32). For quadrupole focusing in the wiggle plane (hence defocusing in y) $k_{\beta x} = k_q$ from Eq. (15) and $k_{\beta y} = \tilde{k}_\beta$ from Eq. (18). For a helical wiggler

$$k_{\beta x} = k_{\beta y} = \frac{b_0}{2\gamma k_w} \quad . \qquad (46)$$

The electron motion is fully 3-dimensional, clearly. The laser field, however, is assumed to be 2-dimensional; for ATA simulations, the laser field is assumed to be cylindrically symmetric, and the two dimensions are r and z.

The field is solved in the paraxial approximation.[7] The electric field - linearly polarized, for a linear wiggler - is written

$$E_x(x,y,z,t) = R_e \left[\mathcal{E}(x,y,z) \, e^{\, i \, (k \, z \, - \, \omega \, t)} \right] \quad , \qquad (47)$$

where $\mathcal{E}$ is a slowly varying, complex electric field amplitude: the equation

$$\mathcal{E} \equiv |\mathcal{E}| e^{i\phi} \qquad (48)$$

defines ϕ, the phase of the electric field. The code can also simulate a helical wiggler FEL; the modifications to the field equations are straightforward.

With the slowly-varying amplitude and phase approximation, the wave equation becomes

$$\nabla^2 E_x - \frac{1}{c^2} \frac{\partial^2 E_x}{\partial t^2} = e^{i(k \, z \, - \, \omega \, t)} \left(2ik \frac{\partial}{\partial z} + \nabla_\perp^2 \right) \mathcal{E}$$

$$= \frac{4\pi}{c^2} \frac{\partial}{\partial t} J_x \quad . \qquad (49)$$

In cylindrical symmetry

$$\nabla_\perp^2 = \frac{1}{r} \frac{\partial}{\partial r} r \frac{\partial}{\partial r} \quad . \qquad (50)$$

For the source term - the right-hand side of Eq. (49) - we assume that only the Fourier component of J_x proportional to $e^{i(k \, z \, - \, \omega t)}$ contributes to the field evolution. Implicit is the approximation that the field changes little over many optical wavelengths.

Defining,

$$\frac{e \, \mathcal{E}}{\sqrt{2} m_e c^2} = e_1 + i \, e_2 \equiv e_s \, e^{i\phi} \qquad (51)$$

(the factor of $\sqrt{2}$ ensures that e_1 and e_2 refer to r.m.s. values), and writing

$$J_x(x,y,z) = -e\sum_i v_{x_i}\,\delta(y - y_i)\,\delta(z - z_i)$$

with

$$v_{xi} = c\frac{\sqrt{2}a_w}{\gamma_i}e^{-ik_w z_i}\ , \qquad (52)$$

we obtain[6]

$$(2ik\frac{\partial}{\partial z} + \nabla_\perp^2)(e_i + ie_2) \simeq \frac{4\pi i\omega e\, a_w f_B}{m_e c^4}\,\frac{I}{N}\sum_i \frac{e^{-i\theta_i}}{\gamma_i}\,\delta(x - x_i)\delta(y - y_i) \qquad (53)$$

Here I is the beam current and N the number of simulation particles; I/N is therefore the current per particle. The field quantities e_1 and e_2 are both functions of x, y, and z.

To solve Eq. (54) numerically, we integrate both sides over radial zones of width Δr(in general Δr varies with r). Then, at a radial grid point,

$$(2ik\frac{\partial}{\partial z} + \nabla_\perp^2)(e_i + ie_2) \simeq \frac{2i\omega e\, a_w f_B}{m_e c^4}\,\frac{I}{N}\,\frac{1}{r\Delta r}\sum_i \frac{e^{-i\theta_i}}{\gamma_i} \qquad (54)$$

where now the sum is only over the particles lying within the radial zone Δr around the grid point.

Equation (54) is solved using a finite element method, which permits a unique weighting of particles to radial grid points.

We present the results of three simulations for a 24 m wiggler on ATA. The three simulations differ only by type of wiggler - helical, linear with external quadrupole focusing, and linear with wiggle plane focusing due to

parabolic pole faces. In all three cases, the wiggler is tapered in a_w according to the usual self-design procedure: a design electron, in a circular orbit at r_{design}, is maintained at a fixed $\psi_r = 0.35$ as the electron is decelerated. The other parameters for all three runs are

$\gamma = 98.85$	
$\epsilon_N = 0.14$ rad cm	(normalized edge emittance for a parabolic beam profile).
$P_{in} = 2.4$ GW	(laser input power)
$I = 2$ kA	
$\mathscr{J} = 2.10^5$ A cm^{-2}	(electron beam brightness, defined as $\mathscr{J} \equiv \pi^2 I/\gamma^2 V_4$, where V_4 is the volume of the 4-dimensional transverse phase space occupied by the electron beam).
$\omega_0 = 0.35$ cm	(laser beam waist)
$\lambda_w = 8$ cm	(wiggler wavelength)
$\lambda_s = 10.6$ μm	(signal wavelength) .

In all three cases, the beam waist occurs 0.5 Rayleigh ranges before the wiggler; the entering laser beam is diverging. Figures 3a - 3c show the calculated laser power as a function of z in the wiggler; the third case (Fig. 3c) with quadrupole focusing sufficient to keep the electron beam circular, performs approximately half as well as the helical wiggler (Fig. 3a) or the linear wiggler with parabolic pole faces (Fig. 3b). The reason for the poor performance can be seen in Figs. 4a - 4c; these are histograms of final electron distributions in γ. The linear wiggler with quadrupole focusing has

permitted a very much smaller final trapping fraction; considerable electron detrapping occurred as the bucket moved between $\gamma \approx 96$ and $\gamma \approx 84$.

The linear wiggler with parabolic pole faces did not perform quite as well as the helical wiggler; the Bessel function factor f_B readily explains the difference.

V. QUALIFICATIONS

We stress that the numerical simulations follow the betatron motion of the electrons separately from the wiggle motion; the betatron equations in the simulations are Eq. (45), not the full equations of motion, Eqs. (26). There are many potential resonances and couplings between (for example) wiggle and betatron motion that cannot be examined in the current version of the code. The full equations of motion will shortly be put into the code, permitting a better numerical examination of electron transport in the wiggler.

REFERENCES

1. V. K. Neil, SRI Tech. Rept. JSR-79-10 (1979); see also C. M. Tang, NRL Memorandum 4820 (1982).
2. N. M. Kroll, P. L. Morton, and M. N. Rosenbluth, IEEE Journal Quantum Electronics 17, 1436 (1981).
3. W. M. Fawley, D. Prosnitz, and E. T. Scharlemann, UCRL-90838 and Phys. Rev. A, to be published (1984).
4. D. Prosnitz and E. T. Scharlemann, ELF Note 86.
5. L. D. Landau and E. M. Lifshitz, Mechanics (Pergamon, NY, 1976) p. 93.
6. W. B. Colson, IEEE Journal Quantum Electronics, 17, 1417 (1981).
7. J. H. Marburger, Prog. Quant. Electronics, 4, 35 (1975).

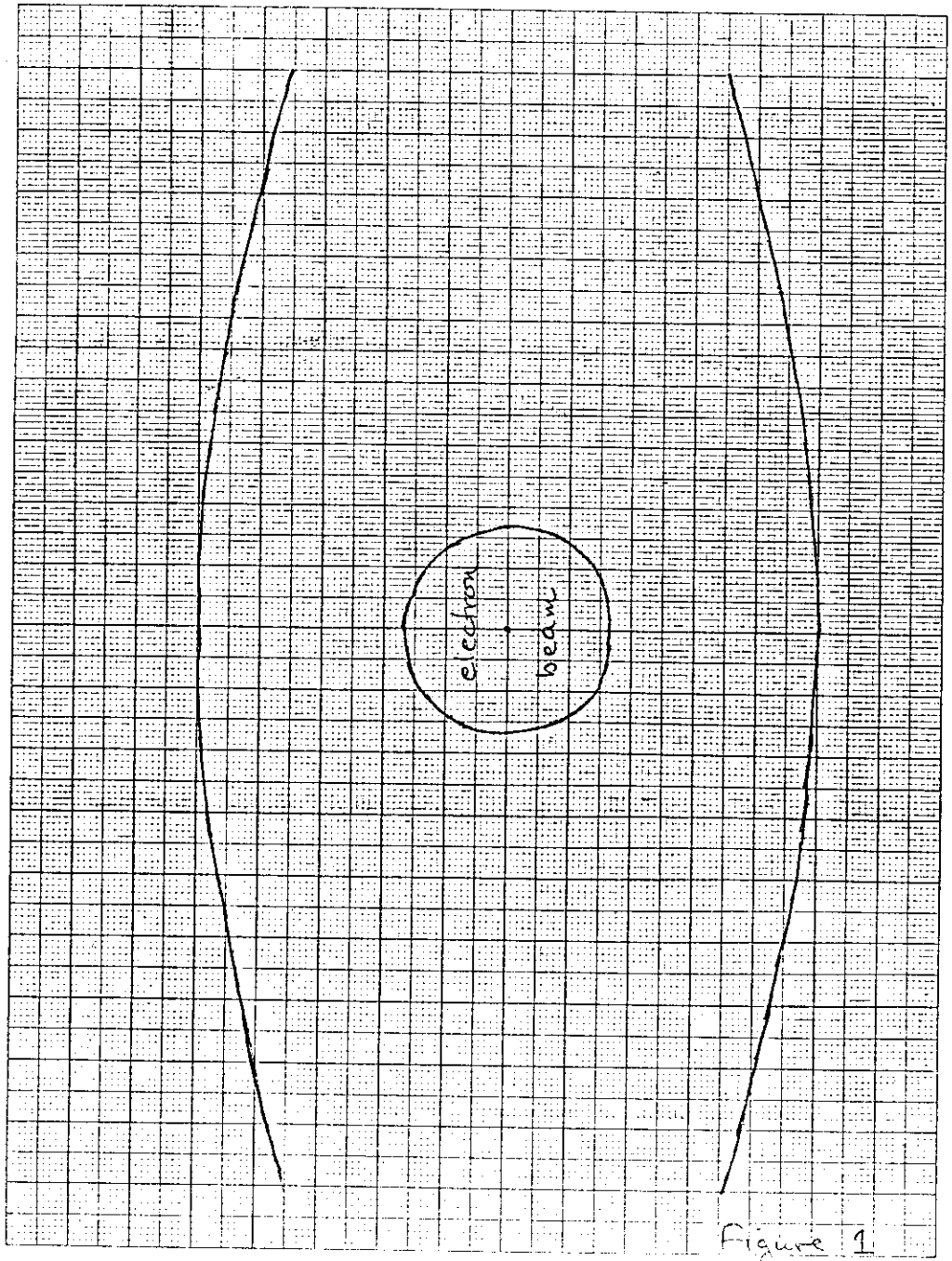

Figure 1

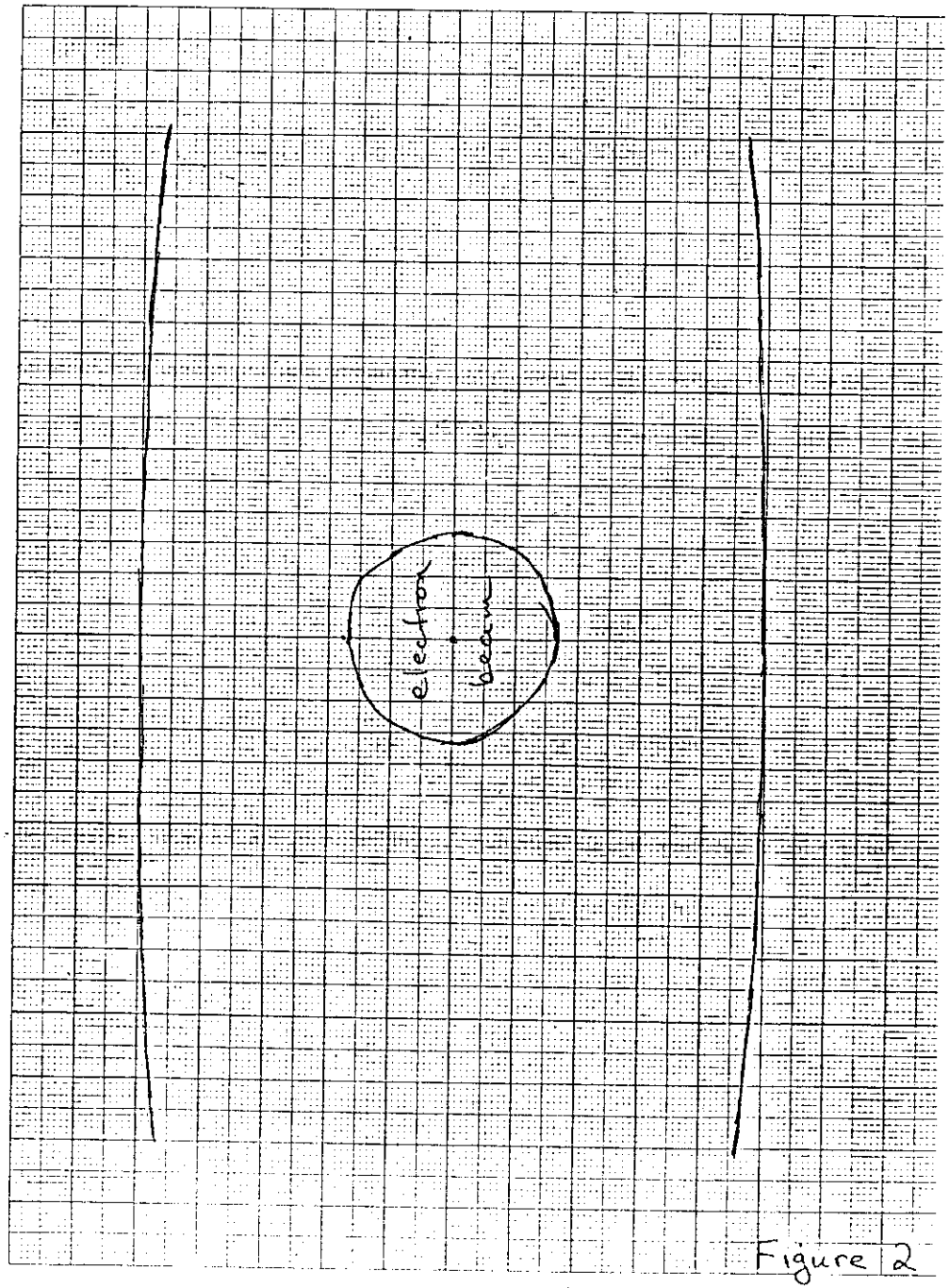

Figure 2

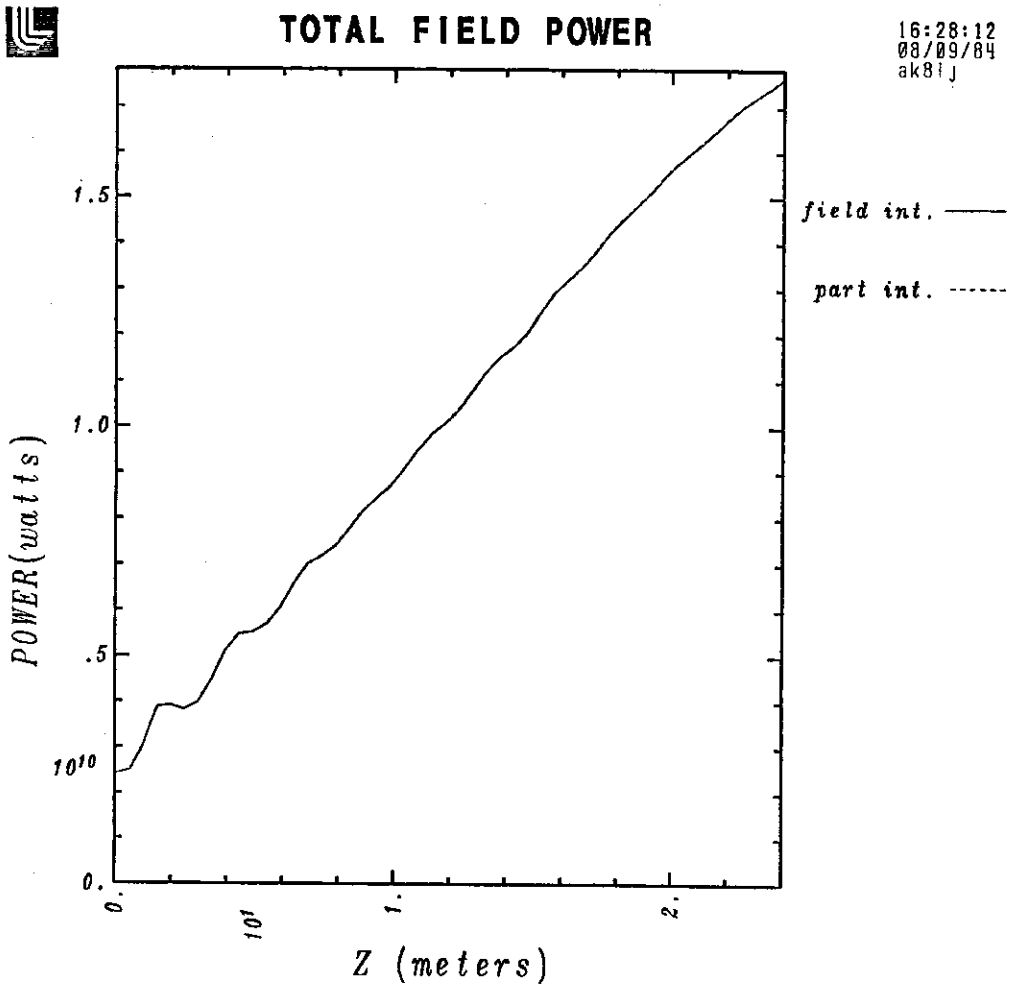
TOTAL FIELD POWER
16:28:12
08/09/84
ak8ij
field int.
part int.
POWER(watts)
1.5
1.0
.5
10^{10}
0.
0.
10^{1}
1.
2.
Z (meters)

Fig 3a

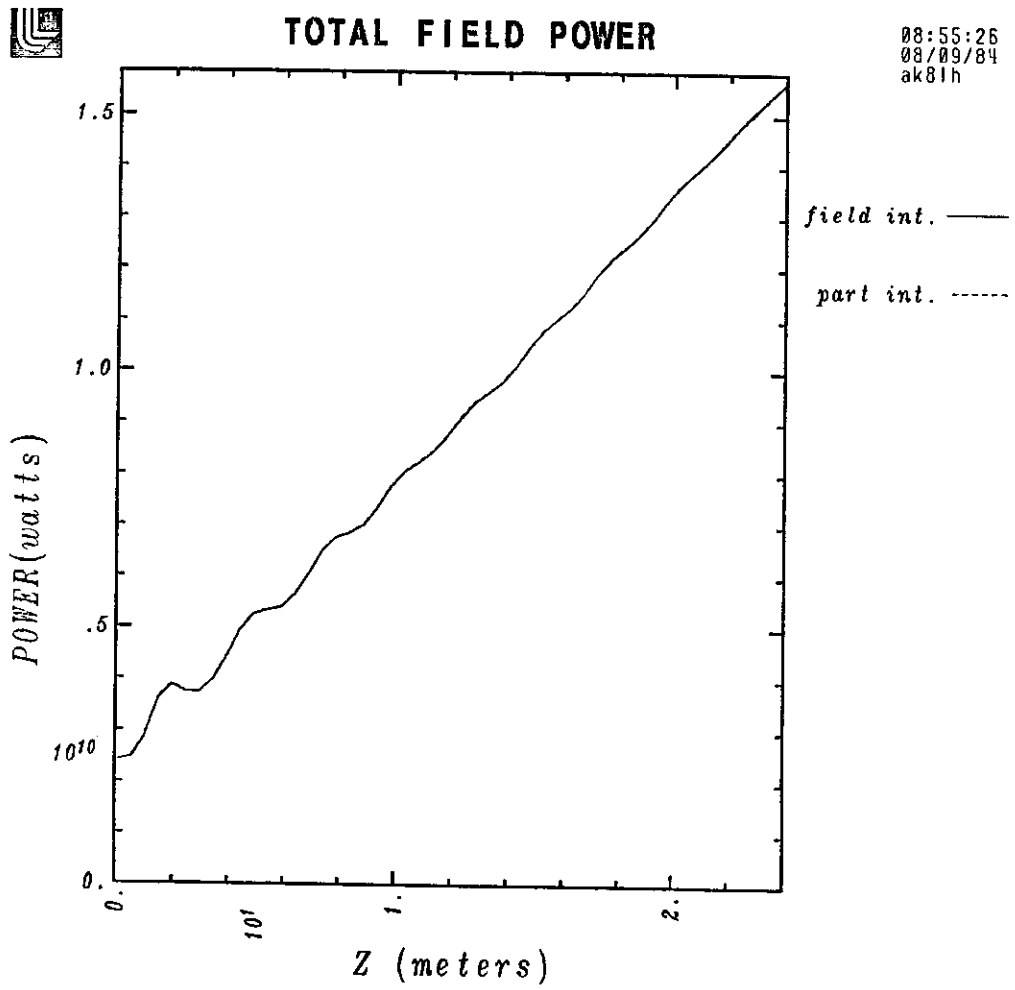
TOTAL FIELD POWER
08:55:26
08/09/84
ak8ih
field int.
part int.
POWER(watts)
1.5
1.0
.5
10^{10}
0.
0.
10^{1}
1.
2.
Z (meters)

Fig. 3b

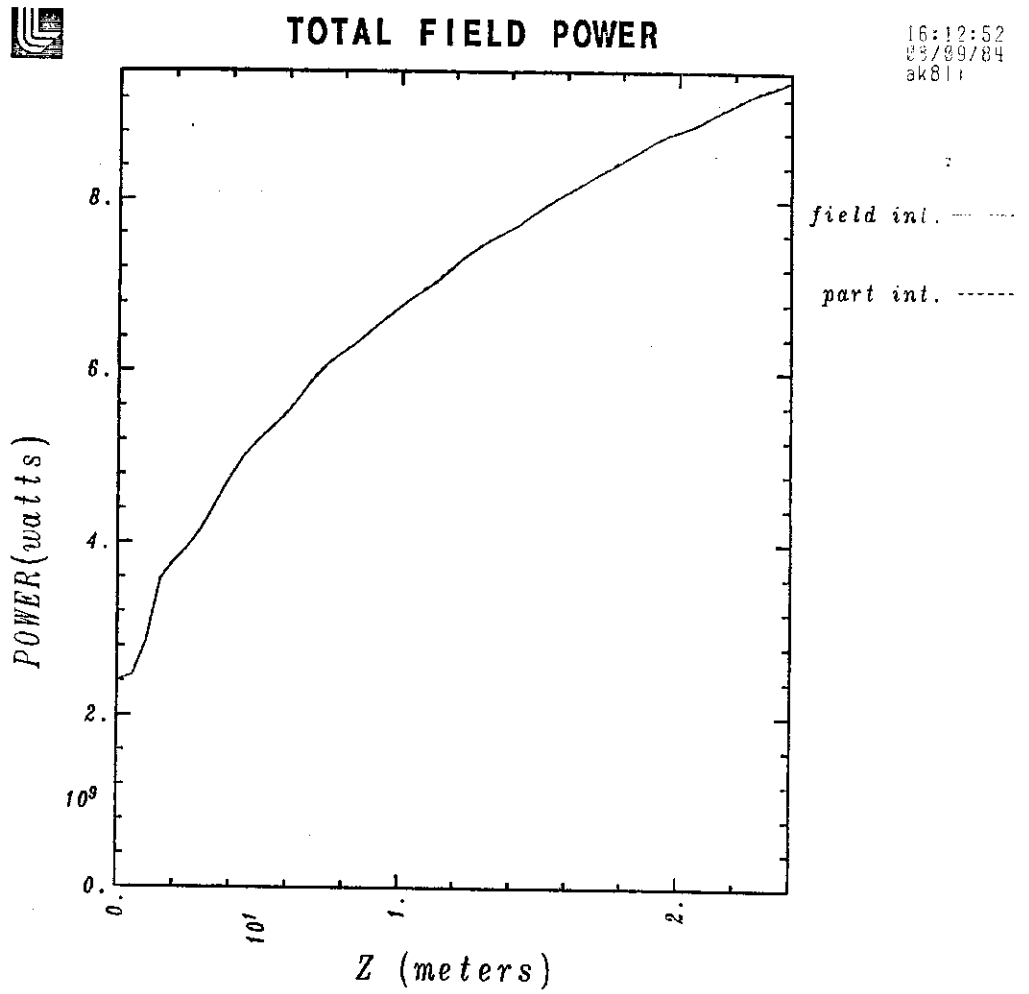
TOTAL FIELD POWER
16:12:52
08/09/84
ak81i
field int.
part int.
POWER(watts)
8.
6.
4.
2.
10⁰
0.
0.
10¹
1.
2.
Z (meters)

Fig. 3c

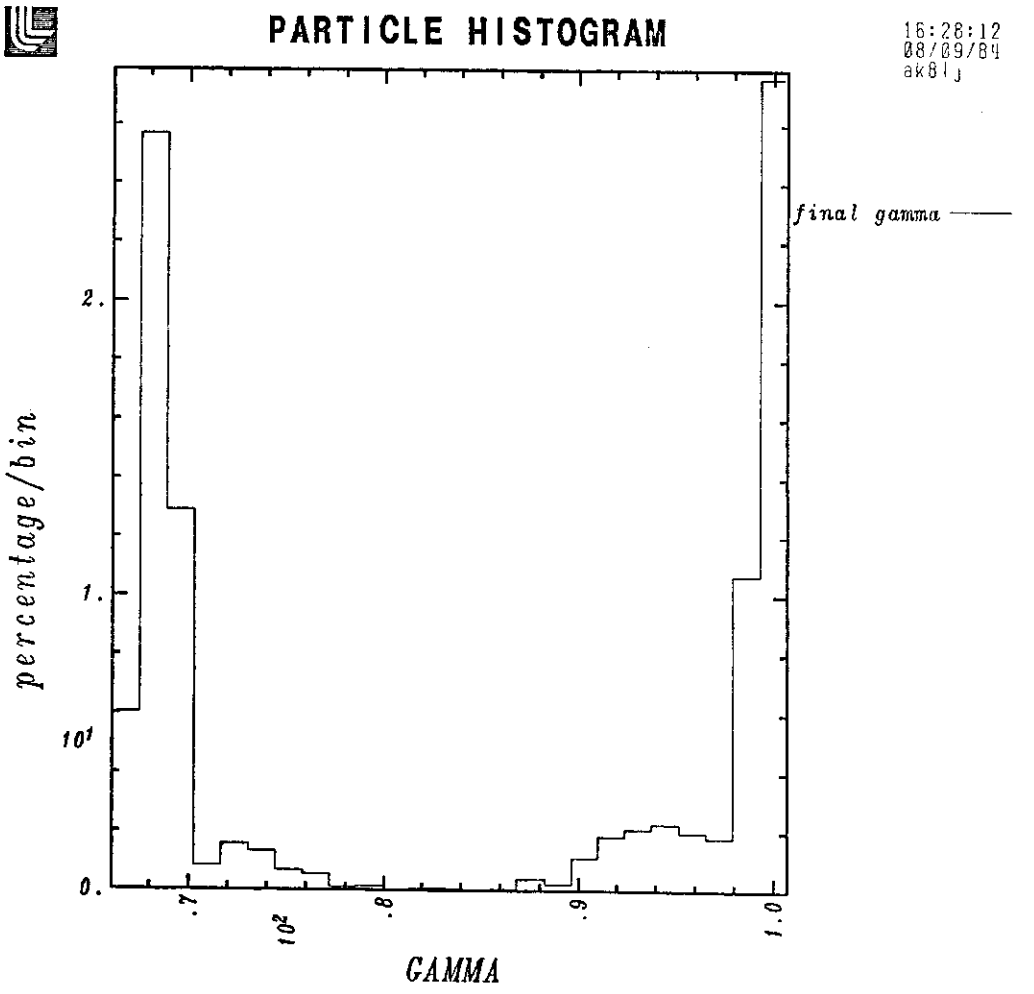
PARTICLE HISTOGRAM
16:28:12
08/09/84
ak81j
final gamma
percentage/bin
2.
1.
10¹
0.
.7
10²
.8
.9
1.0
GAMMA

Fig. 4a

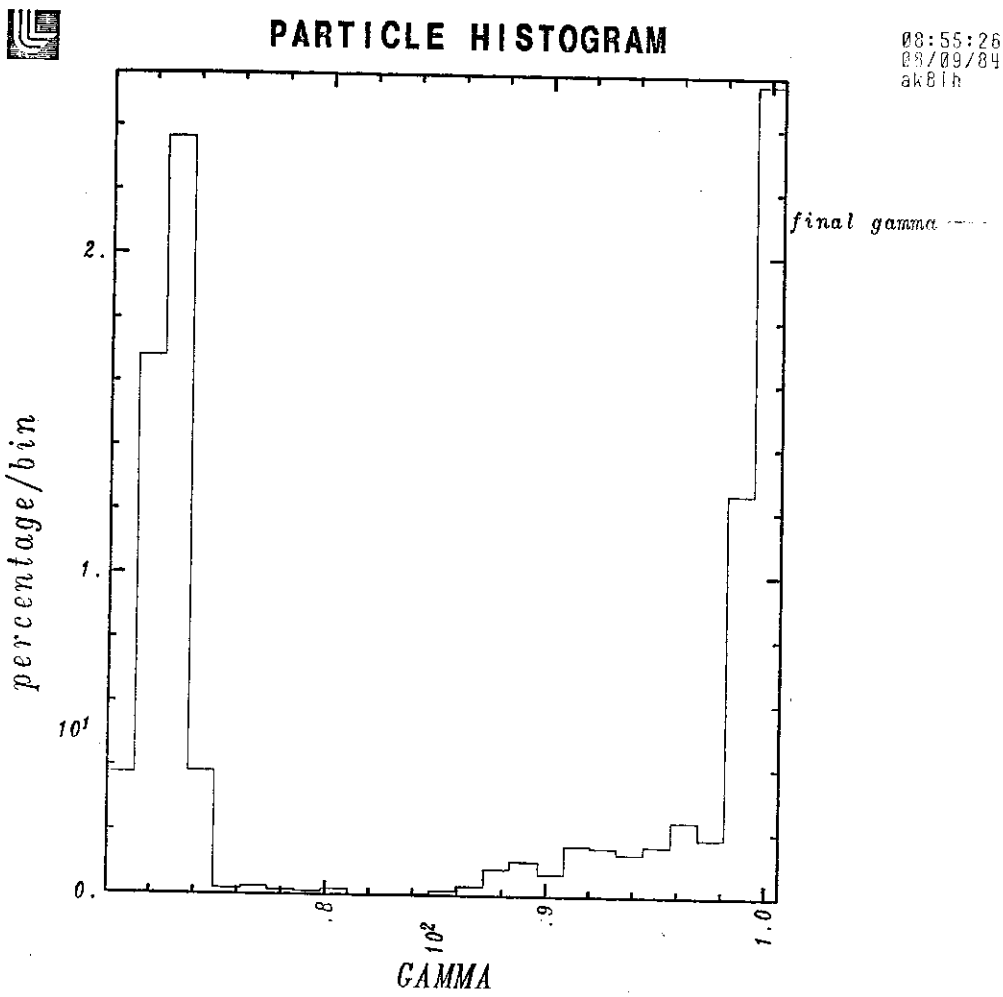
PARTICLE HISTOGRAM
08:55:26
08/09/84
ak8ih
final gamma
percentage/bin
2.
1.
10¹
0.
.8
10²
.9
1.0
GAMMA

Fig. 4b

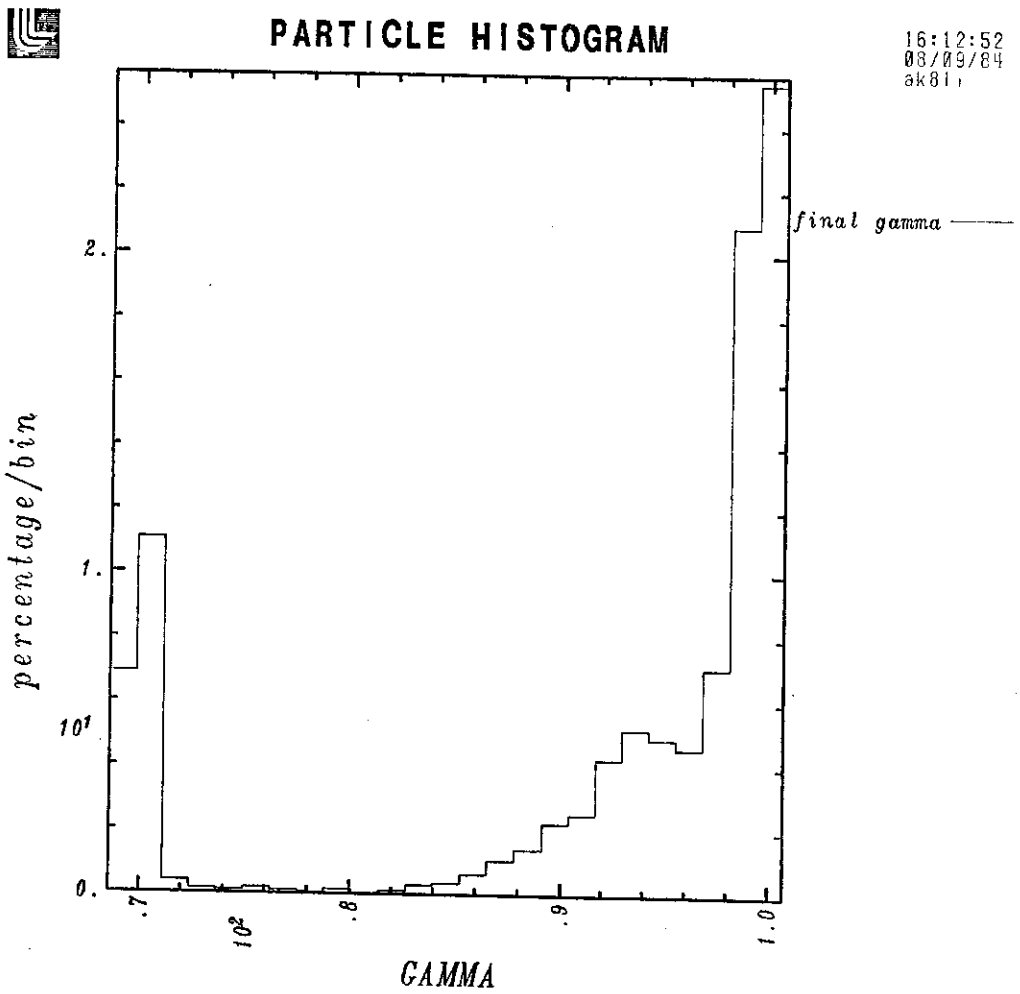
PARTICLE HISTOGRAM
16:12:52
08/09/84
ak8i
final gamma
percentage/bin
2.
1.
10¹
0.
.7
10²
.8
.9
1.0
GAMMA

Fig. 4

OPTICAL GUIDING IN A FREE ELECTRON LASER

E. T. Scharlemann
University of California
Lawrence Livermore National Laboratory*
Post Office Box 808/L-321
Livermore, CA 94550

A. M. Sessler and J. S. Wurtele**
Lawrence Berkeley Laboratory+
One Cyclotron Road/58-101
Berkeley, CA 94720

October 16, 1984

ABSTRACT

The coherent interaction between an optical wave and an electron beam in a free electron laser (FEL) is shown to be capable of optically guiding the light. The effect is analyzed using a two-dimensional approximation for the FEL equations, and using the properties of optical fibers. Results of two-dimensional (cylindrically symmetric) numerical simulations are presented, and found to agree reasonably well with the analytically derived criterion for guiding. Under proper conditions, the effect can be large and has important applications to short wavelength FEL's and to directing intense light.

* Work performed jointly under the auspices of the U. S. Department of Energy by Lawrence Livermore National Laboratory under contract W-7405-ENG-48 and for the Department of Defense under Defense Advanced Research Projects Agency ARPA Order No. 4395 Amendment No. 31, monitored by Naval Surface Weapons Center under document number N60921-84-WR-W0080.

+ This work was supported by the Director, Advanced Energy Systems, Basic Energy Sciences, Office of Energy Research, US DOE under contract number DE-AC03-76SF00098.

** Present Address: Plasma Fusion Center, Massachusetts Institute of Technology

I. INTRODUCTION

It has long been known that the coherent interaction between the light and the electron beam in an FEL produces a phase shift of the light [1], and that the sign of the effect is such that the light is refracted toward the electron beam [1,2]. In recent numerical simulations we have observed guiding of the light by the electron beam, as if the electron beam were an optical fiber [3,4]. These observations stimulated the investigation reported on here.

In this work we treat the bunched electron beam as if it were an optical fiber with a constant index of refraction and a well-defined edge. In Sec. II we review the properties of such step-profile optical fibers for a real or complex index of refraction. In Sec. III, we use one-dimensional FEL theory to evaluate the index of refraction of the electron beam, and present numerical simulations to illustrate optical guiding. We then examine, in Sec. IV, guiding in the exponential growth regime. We find that the intuitive criterion for guiding during exponential growth,

$$\alpha z_r > 1 \quad , \tag{1.1}$$

can be strongly violated. Here the field amplitude grows as $e^{\alpha z}$, and z_r is the Rayleigh length obtained from the electron beam size and light wavelength. The analytical derivations are compared with the results of numerical simulations. Finally, in Sec. V, we mention several potential applications of self-guiding.

II. OPTICAL PROPAGATION IN FIBERS

In this section, we review the salient facts about circular step-profile optical fibers, with emphasis on the LP_{01} mode, the lowest order, linearly polarized mode. This is the mode that the numerical calculations model, and which one would expect to be excited in an FEL with a linear wiggler. We determine the value of the fiber parameter (defined below) necessary for optical guiding.

The usual analysis of step profile fibers [3,4] assumes that the fiber consists of a central core of radius a and index of refraction n, and a cladding of index n_{cl}. In our treatment, the core is the electron beam and the cladding is free space.

We can make the assumption that the fiber is weakly guiding:

$$|n - 1| \ll 1 \quad . \tag{2.1}$$

This inequality is quite good for all cases of interest, and is consistent with the assumption of slowly varying phase of the optical field:

$$\frac{d\phi}{dz} \ll k \quad , \tag{2.2}$$

familiar from FEL theory.

Following Marcuse [4], we consider guided modes with only one transverse electric field component E_x (but both magnetic and electric longitudinal components), for which

$$E_x = AJ_\nu(\kappa r) \begin{pmatrix} \cos(\nu\phi) \\ \sin(\nu\phi) \end{pmatrix}, \quad r < a \quad , \tag{2.3}$$

$$E_x = A \frac{J_\nu(\kappa a)}{H_\nu^1(i\gamma a)} H_\nu^1(i\gamma r) \begin{pmatrix} \cos(\nu\phi) \\ \sin(\nu\phi) \end{pmatrix}, \quad r > a \quad . \tag{2.4}$$

In Eq. (2.3) and (2.4), J_ν and H_ν^1 are Bessel functions and Hankel functions of the first kind, respectively. The arguments of the functions are

$$\kappa = \sqrt{n^2k^2 - \beta^2} \quad , \tag{2.5}$$

$$\gamma = \sqrt{\beta^2 - k^2} \quad , \tag{2.6}$$

$$k = \frac{\omega}{c} \quad , \tag{2.7}$$

and the field is assumed to vary as

$$e^{i(\beta z - \omega t)} \quad . \tag{2.8}$$

Continuity of B_z and E_z at the fiber edge yields the dispersion relation:

$$\frac{\kappa J_{\nu+1}(\kappa a)}{J_\nu(\kappa a)} = \frac{\gamma K_{\nu+1}(\gamma a)}{K_\nu(\gamma a)} \tag{2.9}$$

with

$$(\kappa^2 + \gamma^2)\, a^2 \equiv V^2 = (n^2 - 1)\, k^2 a^2 \quad . \tag{2.10}$$

The quantity V is called the "fiber parameter".

The condition for mode cutoff in a fiber is

$$\gamma a \to 0 \quad . \tag{2.11}$$

In this limit the dispersion relation, Eq. (2.9), simplifies to

$$J_1(V_c) = 0 \quad \text{if } \nu = 0 \quad , \tag{2.12}$$

and

$$J_0(V_c) = 0 \quad \text{if } \nu = 1 \quad . \tag{2.13}$$

In Eq. (2.12) V_c is the value, at cutoff, of the fiber parameter V. Clearly, since increasing V means more zeros of the Bessel functions which satisfy $V_c < V$, the fiber parameter measures the number of guided modes supported by the fiber. Note that from Eq. (2.12) there is no cutoff for the LP_{01} mode. (The first index labels the Bessel function, the second labels the zero's.)

While formally there is no cutoff for the LP_{01} mode, it is incorrect to think of the mode as bound by the fiber for all $V > 0$. To examine this more closely, near cutoff ($\gamma a \ll 1$) the $\nu = 0$ modes satisfy:

$$\gamma a = 1.12 \exp\left(-\frac{J_0(V)}{V J_1(V)}\right) \quad . \tag{2.14}$$

Since the mode amplitude falls off radially as $\exp(-\gamma r)$ for large γr, $1/\gamma$ measures the radial extent of the mode. An examination of Eq. (2.14) shows the mode extends far outside the beam for $V \ll 1$.

For the LP_{01} mode to be considered guided, we will somewhat arbitrarily require that the 1/e point of E_x be within 5 times the fiber radius. This condition corresponds to demanding that

$$V^2 > 1 \quad . \tag{2.15}$$

The analysis can be extended to a fiber with gain (or loss) by permitting V to be complex. The dispersion relation, Eq. (2.9), is unchanged, but κ and γ can now also be complex. From numerical solution of the complex dispersion relation, we find the above criterion (2.15) generalizes to

$$\mathrm{Re}(V^2) + 1/2\ \mathrm{Im}(V^2) > 1 \quad . \tag{2.16}$$

The nature of the solution, however, is different -- a complex γ corresponds to propagation of radiation away from the fiber, balanced by gain in the fiber.

If we examine light propagation in an infinite parabolic medium with gain [5] we obtain an analogous criterion for guiding.

III. THE INDEX OF REFRACTION OF AN ELECTRON BEAM

3.1 General Analysis

The electron beam in a high-gain FEL physically bunches on an optical wavelength; because of the bunching, the beam has an effective index of refraction greater than unity. This is in sharp contrast to the behavior of an unmagnetized (and unbunched) plasma, and is the basis for the optical guiding effects described in this paper. In the previous section, we have presented the criterion that the index of refraction must satisfy in order for a fiber to guide the laser beam; in this section we derive the index of refraction of an electron beam in an FEL.

As a further preliminary, we wish to draw a distinction between two effects, which we will label "refractive guiding" and "gain focusing". The first refers to the familiar guiding of an optical beam by a fiber with a real index of refraction. The power in the optical beam propagates exactly parallel to the fiber. The second, gain focusing, refers to self-similar propagation of an optical beam profile around a fiber with gain: power diffracts away from the fiber, but the gain in the fiber more than balances diffraction. The result is an optical

profile that gr[illegible] in amplitude, but does not change shape (hence the description as self-similar propagation). The distinction between these two cases is primarily in the nature of the index of refraction. Gain focusing occurs around a fiber with a purely imaginary index of refraction; refractive guiding when the index of refraction is purely real. In an FEL, the effective index of refraction is complex, producing a mixture of refractive guiding and gain focusing; in the examples we present, refractive guiding dominates.

Refractive guiding alone dominates in at least two circumstances: a) after saturation in an untapered wiggler (when the light intensity is roughly constant), and b) in a tapered wiggler. The real part of the index of refraction of an optically bunched beam comes from the FEL equations as formulated in Ref. 6:

$$\mathrm{Re}(n)-1 \equiv \frac{1}{k}\frac{d\phi}{dz} = \frac{2\pi e J\, a_w}{mc^3 k e_s} \left\langle \frac{\cos\psi}{\gamma} \right\rangle . \tag{3.1}$$

Gain focusing may dominate in the exponential gain regime of an FEL with an untapered wiggler. The general expression for the imaginary part of the index of refraction comes from the amplitude equation:

$$\mathrm{Im}(n) \equiv \frac{1}{k e_s}\frac{de_s}{dz} = \frac{2\pi e J\, a_w}{mc^3 k e_s} \left\langle \frac{\sin\psi}{\gamma} \right\rangle . \tag{3.2}$$

In Eq. (3.1) and (3.2), e_s is the normalized r.m.s amplitude of the electric field:

$$e_s \equiv \frac{e\,|E_s|}{\sqrt{2}\,mc^2} \tag{3.3}$$

(for a linear wiggler); a_w is the dimensionless r.m.s. vector potential of the wiggler field:

$$a_w \equiv \frac{e\,|B_w|}{\sqrt{2}\,k_w\,mc^2} \tag{3.4}$$

where k_w is the wiggler wavenumber. The current density is J, ψ is the phase of an electron in the pondermotive potential well, and the brackets denote an average over the electron distribution. We use Gaussian c.g.s. units.

From Eq. (3.1) and (3.2) we see that refractive guiding and gain-focusing are distinguished simply by whether $\left\langle \frac{\cos\psi}{\gamma} \right\rangle$ or $\left\langle \frac{\sin\psi}{\gamma} \right\rangle$ dominates; i.e., by the relative phase between the electron bunches and the laser electric field.

The expressions for n in Eq. (3.1) and (3.2) are derived for a uniform infinite medium and a plane electromagnetic wave. We use the value of the index on the electron beam axis to determine the fiber parameter V. The relationships among $d\phi/dz$, de_s/dz and n are changed by two-dimensional effects, as described in Sec. IV.

3.2 Examples of FEL Guiding

In this section, we present numerical simulations to illustrate guiding in the exponential gain regime (which we discuss in detail in Sec. IV), and guiding in an untapered wiggler after saturation. The

simulations were performed at LLNL with the 2-dimensional FEL code FRED. An earlier version of the code is described in Ref. [7] and [8]; the code has since been modified to include full betatron motion of the electrons. The code follows an axisymmetric laser beam around an electron beam that bunches longitudinally (in ψ [1]). Axisymmetric diffraction effects are fully included, via the paraxial wave approximation; refractive and gain effects are included through the local source terms provided by the electron beam.

The two categories of FEL guiding can be illustrated with a single simulation, based on the design of an FEL in a storage ring. The parameters of the simulation are listed in Table I. Figure 1 is a three-dimensional contour plot of laser intensity versus r and z. The initial bump in the laser intensity on axis is the input 30 MW laser beam at a focus; guiding is evident in the later growth of the laser field, and in the saturated regime (past 16 m). The guiding is visible more quantitatively in Figs. 2 through 4, which are cross-sections of the laser profile at several values of z. The laser profile is nearly constant over 60 Rayleigh lengths of propagation. Figure 2 is a cross-section in the exponential gain regime, Fig. 3 in the saturated regime, and Fig. 4 at the end of the wiggler. An interesting effect of the guiding is illustrated in Fig. 5, which is a plot of the phase of the electric field versus radius at the end of the wiggler: the decrease in ϕ with increasing r indicates that the output laser beam is actually converging to a focus 8 cm beyond the end of the wiggler.

3.3 Guiding After Saturation

After saturation, the guiding of the light is entirely refractive, and Eq. (3.1) is applicable. We can generally take the bunching term, $\langle(\cos\psi)/\gamma\rangle$, to be $\simeq 1/2\gamma_0$, where γ_0 is the average electron Lorentz factor. $\cos\psi$ must of course remain less than or equal to unity, and perfect bunching at $\psi=0$ never occurs. Then, for the parameters of the simulation, we find

$$\mathrm{Re}(V) \simeq 1 \quad , \tag{3.5}$$

after saturation.

For guiding of the light after saturation, we obtain in general

$$V^2 = \frac{2eI}{mc^3}\,\frac{ka_w}{\gamma_0^2\sigma_s} \gtrsim 1 \quad , \tag{3.6}$$

where I is the total current. With a slight modification, this equation is applicable to tapered wiggler amplifiers; the expression for V^2 must be multiplied by $\simeq 2f_{trapped}\cos\psi_r$, where $f_{trapped}$ is the fraction of the electrons trapped in the decelerating ponderomotive potential well [1], and ψ_r is the resonant ψ of an electron that decelerates with the bucket.

IV. GUIDING IN THE EXPONENTIAL GAIN REGIME

We can analyze the guiding in the exponential gain regime by extending the linear analysis in Ref. [9] to include the effects of diffraction (and incidentially, energy spread). To do so, we write the longitudinal

electron equations derived by Kroll, Morton, and Rosenbluth [1] in complex form:

$$\frac{d\gamma_j}{dz} = \mathrm{Re}\left[i \frac{a_w f_B}{\gamma_j} e_s e^{i\theta_j} \right] , \tag{4.1}$$

$$\frac{d\theta_j}{dz} = \mathrm{Re}\left[k_w - \frac{k}{2\gamma_j^2} (1 + a_w^2) - \frac{a_w f_B e_s}{\gamma_j^2} e^{i\theta_j} \right] . \tag{4.2}$$

In Eq. (4.1) and (4.2), θ_j is the phase of an electron with respect to a plane wave; in terms of ψ_j and ϕ,

$$\theta_j \equiv \psi_j - \phi . \tag{4.3}$$

The factor f_B is the well-known difference of Bessel functions [10].

The complex field equation follows from Eq. (3.1) and (3.2), but with addition of a transverse gradient term:

$$\frac{\partial e_s}{\partial z} = \frac{2\pi i e a_w}{mc^3} f_B \frac{J}{N} \sum_j \frac{e^{i\theta_j}}{\gamma_j} + \frac{i\nabla_\perp^2 e_s}{2k} , \tag{4.4}$$

where e_s is now a complex field amplitude. The total number of electrons is N. The transverse gradient term follows directly from the paraxial wave equation [11]. The recognition that a guided laser field propagates with an unchanged profile permits us to approximate the transverse gradient term very simply:

$$\frac{\nabla_\perp^2 e_s}{2k} \simeq - \frac{e_s}{z_r} \tag{4.5}$$

where $z_r \equiv kw^2/2$ for a Gaussian profile with an electric field 1/e radius of w. The self-similar profile of a guided beam is not Gaussian; hence the approximate nature of Eq. (4.5).

Equations (4.1), (4.2), and (4.4) can now all be linearized, taking e_s to vary as $e^{j\lambda(z/zr)}$. To incorporate an electron energy spread, we take a square distribution for the electron energy:

$$f(\gamma) = \frac{1}{2\Delta\gamma} , \quad \gamma_0 - \Delta\gamma \le \gamma \le \gamma_0 + \Delta\gamma$$
$$= 0 , \quad \text{otherwise.} \tag{4.6}$$

The result of linearization is a cubic in the complex, dimensionless parameter λ:

$$\lambda^3 + \lambda^2 [1 + 2\Delta k_0 z_r]$$
$$+ \lambda \left[2\Delta k_0 z_r + (\Delta k_0 z_r)^2 - 4(k_w z_r)^2 \frac{\Delta\gamma^2}{\gamma_0^2} \right] \tag{4.7}$$
$$+ A k_w z_r + (\Delta k_0 z_r)^2 - 4(k_w z_r)^2 \frac{\Delta\gamma^2}{\gamma_0^2} = 0 .$$

Here

$$\Delta k_0 \equiv k_w - \frac{k}{2\gamma_0^2} (1 + a_w^2) \tag{4.8}$$

is a parameter that measures the departure from resonance of the center, γ_0, of the electron distribution function, and

$$A \equiv \frac{4\pi e J}{mc^3} \frac{a_w^2 f_B^2}{\gamma_0^3} z_r^2 \tag{4.9}$$

is the dimensionless parameter that measures the coupling between the electron beam and the light.

One's natural inclination is to attempt a simplification of this cubic, identifying the dominant terms and discarding the rest. Unfortunately, for many applications, all terms in the cubic are comparable, and the standard general expression for the analytic solution to a cubic must be used.

The expression for the fiber parameter V of the electron beam in terms of λ is simple, and comes from Eqs. (3.1), (3.2), (4.4) and (4.5):

$$V^2 = \frac{2ka^2}{z_r} (1 + \lambda) \quad . \tag{4.10}$$

We take the 1/e point of the Gaussian transverse density profile of the electron beam to be an effective fiber radius. For the parameters of the simulation described in Section 3.3, with w=0.02 cm (as observed in the simulation), the cubic yields

$$\begin{aligned} V^2 &= 1.03 - 0.12i \\ \lambda &= 0.03 - 0.12i \end{aligned} \tag{4.11}$$

Our criterion for guiding [Eq. (2.16)] is satisfied, although the laser beam is somewhat more tightly confined to the electron beam than $|V| = 1$ would predict. In terms of either the assumed w, or V, the discrepancy is only about 20 percent.

The value for $|\mathrm{Im}(\lambda)|$ is consistent with the exponential gain observed in the simulation. The fact that $\mathrm{Im}(\lambda)$ is much less than unity indicates that the gain length is much longer than the Rayleigh range,

strongly violating the naive criterion mentioned in the Introduction, Eq. (1.1).

The general procedure for evaluating the importance of guiding laser light by an electron beam is iterative. The cubic, Eq. (4.7), is solved with an assumed value for w; twice the electron beam radius (w=2a) is a good initial guess. From the solution for λ, Eq. (4.10) gives V. The value of V determines, through Eq. (2.9) and (2.10), values for γ and . The quantity w is then given by

$$w = 1/ \ |\mathrm{Re}(\gamma)| \quad . \tag{4.12}$$

Iterating produces a consistent solution for the laser beam size and the growth rate, if a guided solution exists.

We have assumed that the transverse derivative term in Eq. (4.5) can be adequately approximated by using w, the light beam size -- this assumption permitted us to use the Rayleigh range of the laser profile in the derivation. When $w \gg a$, or $V^2 < 1$, this assumption is violated; for $V^2 < 1$, the transverse derivative term must be written as

$$\nabla_\perp^2 e_s = - \kappa^2 e_s \tag{4.12}$$

with κ obtained from the fiber dispersion relation. An interesting example of this limit occurs when the electron beam current becomes very small ($A \to 0$), with $\Delta k_0 = \Delta\gamma = 0$. Then the cubic Eq. (4.7) reduces to

$$\lambda^3 + \lambda^2 + A\, k_w z_r = 0. \tag{4.13}$$

Perturbing around the roots $\lambda = 0, 0, -1$ obtained with $A = 0$, we find

$$= \pm i \sqrt{A k_w z_r}, \quad -A k_w z_r \quad . \tag{4.14}$$

All three roots correspond to $V^2 << 1$ and $w >> a$, as one would expect.

The growing root in Eq. (4.13), $\lambda = -i\sqrt{A k_w z_r}$, is very different from what one would expect from one-dimensional theory, with or without a fill factor. The growth rate is less, and scales as $J^{1/2}$ rather than $J^{1/3}$; the physical reason for the difference is the importance of diffraction in this limit.

As one would expect, diffraction decreases the linear growth rate. The effect of diffraction on guiding is unexpected, however, and can be seen from the form of Eq. (3.1) and (3.2). For a given bunching $\langle(\cos\psi)/\gamma\rangle$, diffraction reduces the electric field e_s. The index of refraction of the electron beam is thereby increased, enhancing the guiding. It is this enhancement that permits exponential gain even when Eq. (1.1) is violated.

V. APPLICATIONS

We have been motivated in this study, and have emphasized in this paper, the importance of optical guiding (under some circumstances) to FEL performance. As we have seen, the phenomena can be rather important and thus one can contemplate FEL's of exceedingly long length. In this way, it appears possible to have a small electron beam radius and a very long wiggler (hence a very high gain FEL) even in the VUV range.

Because of the effect of optical guiding it is possible to direct and focus the FEL-generated-optical beam. This is of interest for very intense beams, such as are contemplated for laser inertial fusion, where lenses and mirrors of conventional materials would be destroyed by the light. Use of optical guiding appears to be relatively straightforward since a simple magnetic deflection of the electron beam will result in a deflection of the light.

It should be noted that optical guiding applies, also, to very short wavelength light, which does not interact coherently with normal material. Application of this to the VUV and to soft X-rays would appear to make possible some interesting devices.

Optical guiding will be effective in an Inverse Free Electron Laser (IFEL) as well as in an FEL (A. Gaupp, private communication) and hence can be important in the operation of an IFEL, but this requires a large accelerated current.

Finally, we note that optical guiding may make possible resonant ring FEL's (J. D. Dawson, private communication). This requires FEL operation when the FEL is no longer straight, which can be achieved with an isochronous ring. It appears possible, in principle, to have an FEL whose gain is modest per unit length, but whose action extends over many circuits of the ring.

After the completion of this work our attention was drawn to work by G. T. Moore which nicely compliments that presented here [12].

Acknowledgements

We are happy to acknowledge useful conversations with W. M. Fawley, K-J Kim, G. Moore, D. Prosnitz and participants at The Workshop on Plasmas, Accelerators, and Free Electron Lasers at the Aspen Center for Physics, 1984, in particular J. M. Dawson, G. Schmidt, and C-M Tang. We also thank the Aspen Center for Physics where part of this work took place.

Table I

Simulation Parameters

Current (I)	270 A
Electron beam radius in the wiggler (a)	0.01 cm
Electron Lorentz factor (γ_0)	2000
Fractional electron energy spread (r.m.s. $\frac{\Delta\gamma}{\gamma}$)	$1.2 \cdot 10^{-3}$
Laser wavelength ($2\pi/k$)	2500 Å
Input laser power	30 MW
Dimensionless r.m.s. wiggler vector potential (a_w)	4.352
Wiggler length	30 m
Wiggler period ($2\pi/k_w$)	10 cm

REFERENCES

[1] W. M. Kroll, P. L. Morton and M. W. Rosenbluth, IEEE Journal of Quantum Electronics, QE-17, 1436 (1981).

[2] C-M Tang and P. Sprangle, "The Three-Dimensional Non-Linear Theory of the Free-Electron-Laser Amplifier," in Free Electron Generators of Coherent Radiation, Physics of Quantum Electroncs 9, Addison-Wesley, Reading, Mass. (1982), p. 627; also personal communication from C-M Tang.

[3] A. W. Snyder and J. D. Love, Optical Waveguide Theory, Chapman and Hall, London (1983).

[4] D. Marcuse, Theory of Dielectric Waveguides, Academic Press, New York and London (1974).

[5] A. Yariv, Introduction to Optical Electronics, 2nd ed., Holt, Rinehart, and Winston, New York, (1971).

[6] D. Prosnitz, A. Szoke and V. K. Neil, Phys. Rev. A 24, 1436 (1981).

[7] W. M. Fawley, D. Prosnitz, S. Doss, and R. Gelinas, "Radially Resolved Simulation of a High-Gain Free Electron Laser Amplifier," in Free Electron Generators of Coherent Radiation, Proc SPIE 453, 212 (1984).

[8] W. M. Fawley, D. Prosnitz, E. T. Scharlemann, "Synchrotron-Betatron Resonances in Free-Electron Lasers," Lawrence Livermore National Laboratory UCRL-90838, to be published in Phys. Rev. A (1984).

[9] R. Bonifacio, C. Pellegrini, and L. M. Narducci, Optics Communications 50, 373 (1984).

[10] W. B. Colson, IEEE Journal of Quantum Electronics, QE-17, 1417 (1981).

[11] J. H. Marburger, Prog. Quantum Electr. 4, 35 (1975).

[12] G. T. Moore, "The High-Gain Regime of the Free-Electron Laser," these proceedings.

FIGURE CAPTIONS

Figure 1. A three-dimensional plot of laser intensity vs. r and z inside the wiggler.

Figure 2. A cross-section of the laser intensity, with a least-squares Gaussian fit, at z = 10 m, in the exponential gain regime. The 1/e point of the electric field for the Gaussian fit (the light beam radius) is at 0.024 cm .

Figure 3. A cross-section of the laser intensity, with a least-squares Gaussian fit, at z = 25 m, after saturation. The light beam radius is 0.023 cm.

Figure 4. A cross-section of the laser intensity, with a least-squares Gaussian fit, at z = 30 m, the end of the wiggler. The light beam radius is 0.024 cm.

Figure 5. A cross-section of the phase ϕ of the complex electric field amplitude at the end of the wiggler, z 30 m, with a least-squares parabolic fit The decrease of ϕ with increasing r indicates that the light is <u>focusing</u> at the end of the wiggler.

8559v/0196v

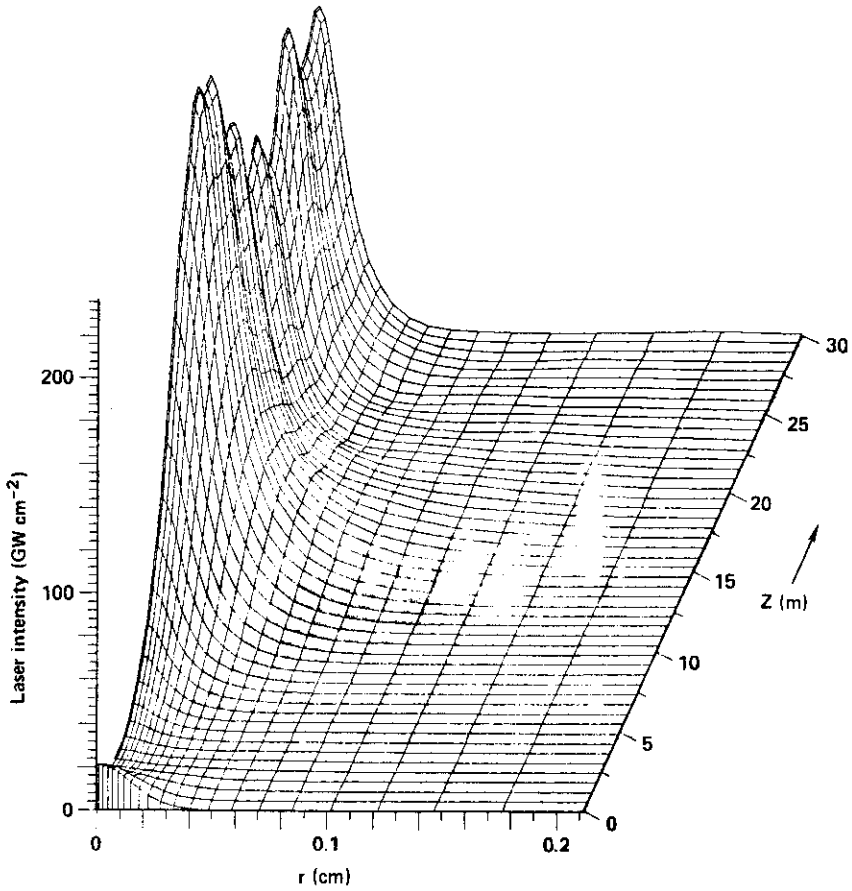

Figure 1

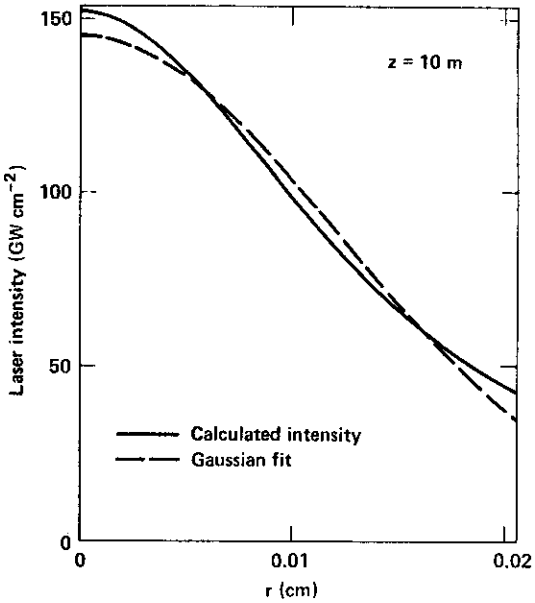

Figure 2

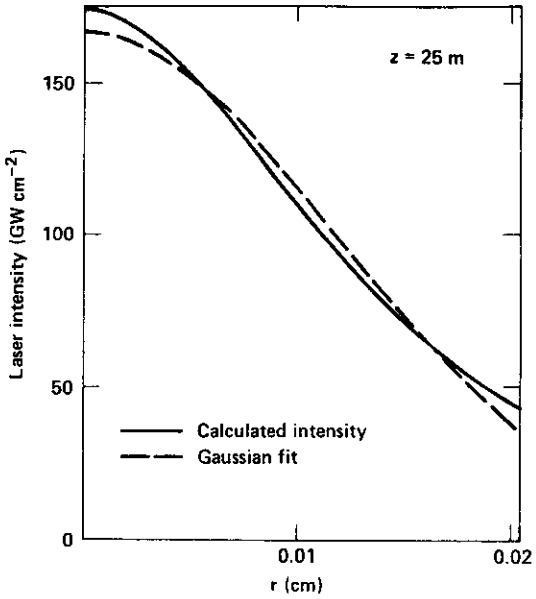

Figure 3

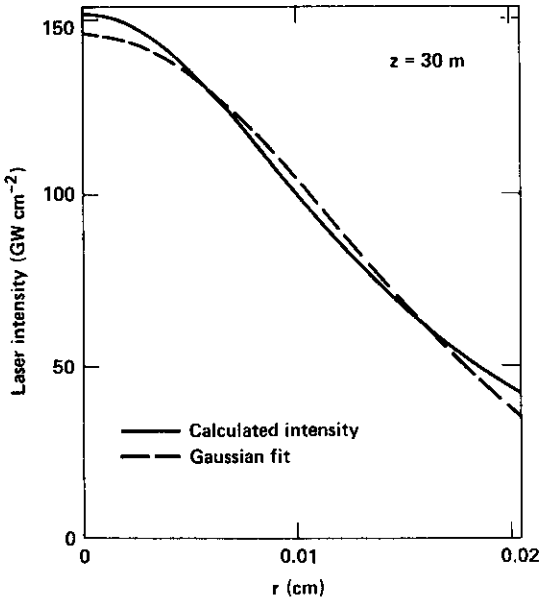

Figure 4

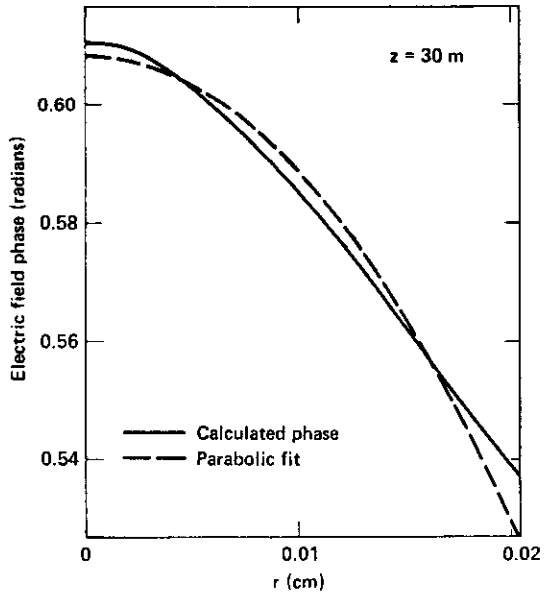

Figure 5